J|A|C|S
ARTICLES

Published on Web 04/09/2010

Enhanced Ion Anisotropy by Nonconventional Coordination Geometry: Single-Chain Magnet Behavior for a [{Fe^{II}L}$_2${$Nb^{IV}(CN)_8$}] Helical Chain Compound Designed with Heptacoordinate Fe^{II}

Thengarai S. Venkatakrishnan,[†,‡] Shaon Sahoo,[§,#] Nicolas Bréfuel,[†,‡] Carine Duhayon,[†,‡] Carley Paulsen,*[,||] Anne-Laure Barra,*[,⊥] S. Ramasesha,*[,§] and Jean-Pascal Sutter*[,†,‡]

CNRS, LCC (Laboratoire de Chimie de Coordination), 205, route de Narbonne, F-31077 Toulouse, France, Université de Toulouse, UPS, INPT, LCC, F-31077 Toulouse, France, Solid State and Structural Chemistry Unit, Indian Institute of Science, Bangalore 560012, India, Institut Néel, CNRS, 25 rue des Martyrs, F-38042 Grenoble, France, Laboratoire National des Champs Magnétiques Intenses (LNCMI), CNRS, 25 rue des Martyrs, F-38042 Grenoble, France, and Department of Physics, Indian Institute of Science, Bangalore 560012, India

Received October 25, 2009; E-mail: sutter@lcc-toulouse.fr; ramasesh@sscu.iisc.ernet.in; carley.paulsen@grenoble.cnrs.fr; anne-laure.barra@grenoble.cnrs.fr

Abstract: Nonconventional heptacoordination in combination with efficient magnetic exchange coupling is shown to yield a 1-D heteronuclear {$Fe^{II}Nb^{IV}$} compound with remarkable magnetic features when compared to other Fe(II)-based single chain magnets (SCM). Cyano-bridged heterometallic {3d-4d} and {3d-5d} chains are formed upon assembling Fe(II) bearing a pentadentate macrocycle as the blocking ligand with octacyano metallates, $[M(CN)_8]^{4-}$ (M = Nb^{IV}, Mo^{IV}, W^{IV}). X-ray diffraction (single-crystal and powder) measurements reveal that the $[\{(H_2O)Fe(\mathbf{L^1})\}\{M(CN)_8\}\{Fe(\mathbf{L^1})\}]_\infty$ architectures consist of isomorphous 1-D polymeric structures based on the alternation of $\{Fe(\mathbf{L^1})\}^{2+}$ and $\{M(CN)_8\}^{4-}$ units (**L¹** stands for the pentadentate macrocycle). Analysis of the magnetic susceptibility behavior revealed cyano-bridged {Fe−Nb} exchange interaction to be antiferromagnetic with $J = -20$ cm^{-1} deduced from fitting an Ising model taking into account the noncollinear spin arrangement. For this ferrimagnetic chain a slow relaxation of its magnetization is observed at low temperature revealing a SCM behavior with $\Delta/k_B = 74$ K and $\tau_0 = 4.6 \times 10^{-11}$ s. The M versus H behavior exhibits a hysteresis loop with a coercive field of 4 kOe at 1 K and reveals at 380 mK magnetic avalanche processes, i.e., abrupt reversals in magnetization as H is varied. The origin of these characteristics is attributed to the combination of efficient {Fe−Nb} exchange interaction and significant anisotropy of the $\{Fe(\mathbf{L^1})\}$ unit. High field EPR and magnetization experiments have revealed for the parent compound $[Fe(\mathbf{L^1})(H_2O)_2]Cl_2$ a negative zero field splitting parameter of $D \approx -17$ cm^{-1}. The crystal structure, magnetic behavior, and Mössbauer data for $[Fe(\mathbf{L^1})(H_2O)_2]Cl_2$ are also reported.

Introduction

Magnetic supramolecular 1D architectures have received renewed interest since it has been shown that such organizations may exhibit slow reversal of their magnetization below a blocking temperature, T_B, and give rise to magnetic hysteresis.[1−9] Such compounds known as single chain magnets (SCM) have already made it possible to throw light on important dynamic properties predicted by Glauber and are anticipated to exhibit quantum effects of magnetic properties as observed for the related single molecule magnets.[10−14] Moreover, their magnetic bistability positions them as potential candidates for future high-density data storage materials.[15] Two main requirements for observing SCM behavior are Ising-type magnetic anisotropy and negligible magnetic interactions between the chains in the crystal; also, a substantial intrachain exchange interaction is desirable for raising the blocking temperatures. The first

---

[†] Laboratoire de Chimie de Coordination.

[‡] Université de Toulouse.

[§] Solid State and Structural Chemistry Unit, Indian Institute of Science.

[#] Department of Physics, Indian Institute of Science.

[||] Institut Néel.

[⊥] Laboratoire National des Champs Magnétiques Intenses.

(1) Caneschi, A.; Gatteschi, D.; Lalioti, N.; Sangregorio, C.; Sessoli, R.; Venturi, G.; Vindigni, A.; Rettori, A.; Pini, M. G.; Novak, M. A. *Angew. Chem., Int. Ed.* **2001**, *40*, 1760–1763.

(2) Clérac, R.; Miyasaka, H.; Yamashita, M.; Coulon, C. *J. Am. Chem. Soc.* **2002**, *124*, 12837–12844.

(3) Gatteschi, D.; Sessoli, R. *Angew. Chem., Int. Ed.* **2003**, *42*, 269–297.

(4) Lescouëzec, R.; Toma, L. M.; Vaissermann, J.; Verdaguer, M.; Delgado, F. S.; Ruiz-Pérez, C.; Lloret, F.; Julve, M. *Coord. Chem. Rev.* **2005**, *249*, 2691–2729.

(5) Coulon, C.; Miyasaka, H.; Clérac, R. *Struct. Bonding (Berlin)* **2006**, *122*, 163–206.

(6) Bernot, K.; Bogani, L.; Caneschi, A.; Gatteschi, D.; Sessoli, R. *J. Am. Chem. Soc.* **2006**, *128*, 7947–7956.

(7) Bogani, L.; Vindigni, A.; Sessoli, R.; Gatteschi, D. *J. Mater. Chem.* **2008**, *18*, 4750–4758.

10.1021/ja9089389

requirement is met by involving building units that possess a nonzero spin ground state with uniaxial anisotropy; 3d metal ions such as Co(II), Mn(III) are customarily used because of their significant single ion anisotropy. These and others are usually found in an octahedral surrounding. However, both the spin state and the magnetic anisotropy depend on the geometry of the coordination sphere of the metal complexes.[16,17] This opens up the possibility of varying the local magnetic feature of the metal ion by simple coordination chemistry and, possibly, increasing the anisotropy for ions considered as less efficient in an octahedral surrounding. In the present report, a heptacoordinated complex has been used as anisotropic building unit, which had a rather large and negative zero-field splitting parameter D.

Ferro(ferri)-magnetic arrangement between the building units leads to the alignment of the local anisotropy throughout the chain and to the stabilization of the resulting magnetization in a preferred orientation. The strength of the intrachain exchange interaction plays a prominent role in stabilizing the magnetic ground state and determines the energy level of the excited states. Moreover, for 1-D Ising magnets, the relaxation process starts with the reversal of one spin, and this reversal requires crossing an energy barrier, Δ, that is proportional to the exchange interaction, J: $\Delta = 2|J|S^2$ in the small J/D limit or $2S^2\sqrt{(2|JD|)}$ in the large J/D limit (according to $H = -J\sum_{-\infty}^{+\infty} \vec{S}_i \vec{S}_{i+1} + D\sum_{-\infty}^{+\infty} \vec{S}_{i+1}{}^2$).[7,12] Therefore strong exchange interaction is also desirable to increase the activation barrier (Δ) for the magnetization reversal, that determines the relaxation rate of the magnetization.[18,19] Stronger exchange interactions in molecular assemblies have been obtained when 3d spin carriers are replaced by their heavier 4d and 5d congeners. For instance, for Cr^{III}, Mo^{V}, and W^{V} cyano-bridged compounds, an increase of the exchange strength with Ni^{II} has been evidenced following the trend 3d < 4d <5d, the W^{V} derivative exhibiting an exchange coupling twice as large as its 3d homologue Cr^{III}.[20−23] In 3D frameworks, such ions have permitted obtaining magnets with T_c's above 100 K.[24−26] We now have envisaged the use of such heavier ions to increase the exchange parameter in chain compounds with the aim of improving their SCM features. We report here our results on 1D architectures combining octacyanometalates and an anisotropic heptacoordinated $\{Fe^{II}(\mathbf{L^1})\}^{2+}$ unit with $S = 2$ spin state. The assemblage formed with the paramagnetic $\{Nb(CN)_8\}^{4-}$ linker exhibits the anticipated SCM behavior with remarkable characteristics underlining the potential of the heptacoordinated Fe^{II} building unit.

Chart 1. Structure of the $\{Fe(\mathbf{L^1})\}^{2+}$ Unit and ORTEP Plot (50% Probability Level) of the Cationic Unit in the Complex $\{Fe(\mathbf{L^1})(H_2O)_2\}Cl_2 \cdot 4H_2O$[a]

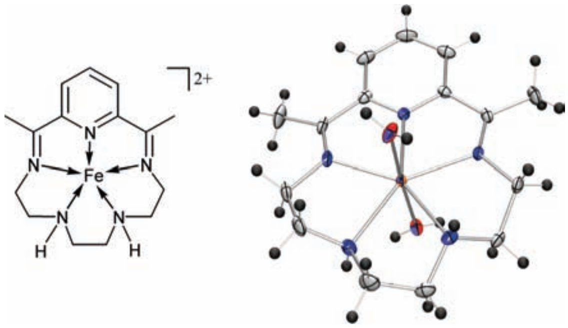

[a] Detailed structural data for this compound are given in the Experimental Section and in Supporting Information.

Results and Discussion

Synthesis and Structural Features. Complexes of paramagnetic 3d ions with all of the equatorial coordination sites blocked by a macrocyclic ligand are well-suited building blocks to form low-dimensional architectures with octacyanometalates.[27−30] Moreover, the dimensionality of the resulting assemblage is dictated by the size of the ligand. For instance, chain organizations have been obtained with the pentadentate macrocyclic ligand $\mathbf{L^1}$ (Chart 1). Considering the design of both the supramolecular organization and the targeted magnetic behavior, we have selected the hepta-coordinated paramagnetic Fe^{II} complex $[Fe(\mathbf{L^1})(H_2O)_2]^{2+}$ and $[Nb(CN)_8]^{4-}$ as complementary modules. The related $[Mo^{IV}(CN)_8]^{4-}$ and $[W^{IV}(CN)_8]^{4-}$ chains have also been prepared, even if these units are diamagnetic; this was done mainly for characterization purposes.

The reactions of $[Fe(\mathbf{L^1})(H_2O)_2]Cl_2 \cdot 4H_2O$ (Chart 1 and Supporting Information) with octacyanometalate $[M^{IV}(CN)_8]^{4-}$ ($M = Nb, Mo, W$) in a $H_2O-EtOH$ mixture yield a 1D cyano-bridged heteronuclear assemblage of formula $[\{(H_2O)Fe(\mathbf{L^1})\}\{M(CN)_8\}\{Fe(\mathbf{L^1})\}]_\infty$ [M = Nb (**1**), Mo (**2**), W (**3**)]. Attempts have been made with the related $[M^{V}(CN)_8]^{3-}$ cyanometalates (M = Mo, W), but the same $\{Fe^{II}{}_2M^{IV}\}$ chains were obtained. Evidently, the group 6 metal (Mo, W) undergoes reduction from M^{V} to M^{IV} during the reaction.

---

(8) Ishii, N.; Okamura, Y.; Chiba, S.; Nogami, T.; Ishida, T. *J. Am. Chem. Soc.* **2008**, *130*, 24–25.
(9) Gatteschi, D.; Sessoli, R.; Villain, J. *Molecular Nanomagnets*; Oxford University Press: Oxford, 2006.
(10) Glauber, R. J. *J. Math. Phys.* **1963**, *4*, 294–307.
(11) Coulon, C.; Clérac, R.; Lecren, L.; Wernsdorfer, W.; Miyasaka, H. *Phys. Rev. B* **2004**, *69*, 132408.
(12) Miyasaka, H.; Julve, M.; Yamashita, M.; Clérac, R. *Inorg. Chem.* **2009**, *48*, 3420–3437.
(13) Wernsdorfer, W.; Clérac, R.; Coulon, C.; Lecren, L.; Miyasaka, H. *Phys. Rev. Lett.* **2005**, *95*, 237203.
(14) Barbara, B. *Inorg. Chim. Acta* **2008**, *361*, 3371–3379.
(15) Leuenberger, M. N.; Loss, D. *Nature* **2001**, *410*, 789–793.
(16) Boca, R. *Coord. Chem. Rev.* **2004**, *248*, 757–815.
(17) Rebilly, J.-N.; Charron, G.; Rivière, E.; Guillot, R.; Barra, A.-L.; Duran Serrano, M.; van Slageren, J.; Mallah, T. *Chem.—Eur. J.* **2008**, *14*, 1169–1177.
(18) Wernsdorfer, W.; Aliaga-Alcalde, N.; Hendrickson, D. N.; Christou, G. *Nature* **2002**, *416*, 406–409.
(19) Ishikawa, N.; Sugita, M.; Wernsdorfer, W. *Angew. Chem., Int. Ed.* **2005**, *44*, 2931–2935.
(20) Shores, M. P.; Sokol, J. J.; Long, J. R. *J. Am. Chem. Soc.* **2002**, *124*, 2279–2292.
(21) Visinescu, D.; Desplanches, C.; Imaz, I.; Bahers, V.; Pradhan, R.; Villamena, F.; Guionneau, P.; Sutter, J. P. *J. Am. Chem. Soc.* **2006**, *128*, 10202–10212.
(22) Sutter, J.-P.; Dhers, S.; Costes, J.-P.; Duhayon, C. *C.R. Chimie* **2008**, *11*, 1200–1206.
(23) Sutter, J.-P.; Dhers, S.; Rajamani, R.; Ramasesha, S.; Costes, J.-P.; Duhayon, C.; Vendier, L. *Inorg. Chem.* **2009**, *48*, 5820–5828.
(24) Ruiz, E.; Rodriguez-Fortea, A.; Alvarez, S.; Verdaguer, M. *Chem.—Eur. J.* **2005**, *11*, 2135–2144.
(25) Tanase, S.; Tuna, F.; Guionneau, P.; Maris, T.; Rombaut, G.; Mathonière, C.; Andruh, M.; Kahn, O.; Sutter, J.-P. *Inorg. Chem.* **2003**, *42*, 1625–1631.
(26) Milon, J.; Daniel, M.-C.; Kaiba, A.; Guionneau, P.; Brandès, S.; Sutter, J.-P. *J. Am. Chem. Soc.* **2007**, *129*, 13872–13878.
(27) Pradhan, R.; Desplanches, C.; Guionneau, P.; Sutter, J.-P. *Inorg. Chem.* **2003**, *42*, 6607–6609.
(28) You, Y. S.; Kim, D.; Do, Y.; Oh, S. J.; Hong, C. S. *Inorg. Chem.* **2004**, *43*, 6899–6901.
(29) Venkatakrishnan, T. S.; Desplanches, C.; Rajamani, R.; Guionneau, P.; Ducasse, L.; Ramasesha, S.; Sutter, J. P. *Inorg. Chem.* **2008**, *47*, 4854–4860.
(30) Rombaut, G.; Golhen, S.; Ouahab, L.; Mathonière, C.; Kahn, O. *J. Chem. Soc., Dalton Trans.* **2000**, 3609–3614.

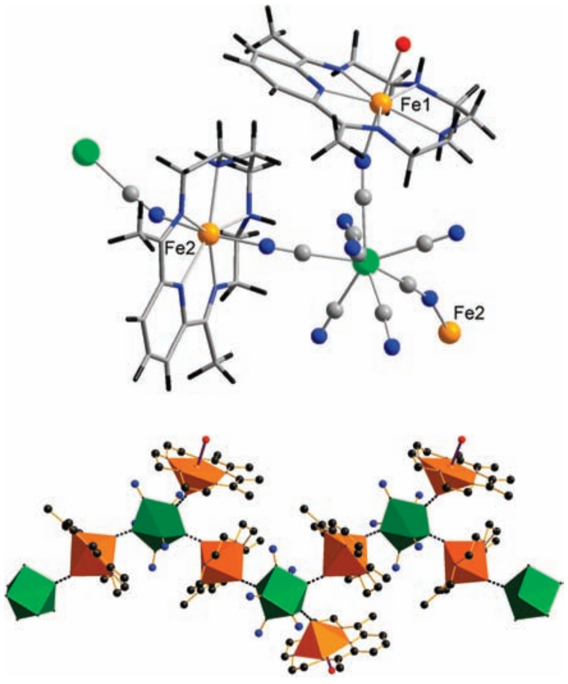

Figure 1. View of the molecular organization of [{(H_2O)Fe($\mathbf{L^1}$)}{$M(CN)_8$}{Fe($\mathbf{L^1}$)}] **1**−**3**. (Top) Asymmetric unit showing the interconnections between the molecular modules. (Bottom) Polyhedral view of the supramolecular chain formed by the alternation of {Fe($\mathbf{L^1}$)} (orange) and {$M(CN)_8$} (green) units.

Slow interdiffusion of the reagent solutions yielded single crystals for all of the compounds, but only those of **2** and **3** were suitable for single-crystal X-ray diffraction studies; those of **1** were not of sufficient quality for X-ray structure determination. The niobium derivative was confirmed to be isostructural to **2** and **3** by its cell parameters[31] and by powder X-ray diffraction (vide infra). The single-crystal X-ray structure determinations revealed that {Fe_2Mo}, **2**, and {Fe_2W}, **3**, have a 1-D polymeric structure based on the alternation of {Fe($\mathbf{L^1}$)} and {$M(CN)_8$} units, an organization isomorphous to the compound formed between {Mn($\mathbf{L^1}$)}$^{2+}$ and {$Nb(CN)_8$}$^{4-}$.[27] A view of the molecular organization is given in Figure 1. Each {$M(CN)_8$}$^{4-}$ is linked by three of its cyanides to three {Fe($\mathbf{L^1}$)} units. One [labeled Fe1 in Figure 1] is terminal, whereas the other two [labeled Fe2 in the structure] accommodate further {$M(CN)_8$} modules in the *trans* position, thus developing the coordination polymer. The structural description made below corresponds to the tungsten chain **3**; the geometrical parameters of **2** are quoted within the brackets. The M−C−N angles are in the range 172.9−178.1° (175.0−178.4° in **2**). The Fe−N−C angles are found to be 158.6° (157.9°) for Fe1 and 152.5° and 160.1° (150.0° and 159.4°), respectively, for the two Fe2 centers linked to the {$M(CN)_8$} unit. The Fe−N(CN) distances are in the range 2.12−2.15 Å, whereas the average Fe−N(pyridine), Fe−N(imine), and Fe−N(H) distances are 2.19, 2.22, and 2.28 Å, respectively. Similar values in bond distances are observed in **2**. These Fe−N bond distances, including those of [Fe($\mathbf{L^1}$)$(H_2O)_2$]$Cl_2\cdot 4H_2O$, are in the range of the distances found for related heptacoordinated Fe complexes[32,33] and in agreement with high-spin Fe(II).[34,35] The Fe(1)−OH_2 distances in **2** and **3** are 2.27(2) and 2.22(2) Å, respectively. The chains adopt a helical arrangement down the *b*-axis and there are both left- and right-handed helixes in the crystal lattice (Figure 2). The packing of the chain in the *bc* plane is such that the alternate chains are running out-of phase, i.e., they are staggered (see Supporting Information). The shortest interchain separation, 3.36 Å, is found between a nitrogen atom of cyanide and the oxygen bound to Fe; the shortest metal−metal distance is 6.80 Å, between Fe1 and W.

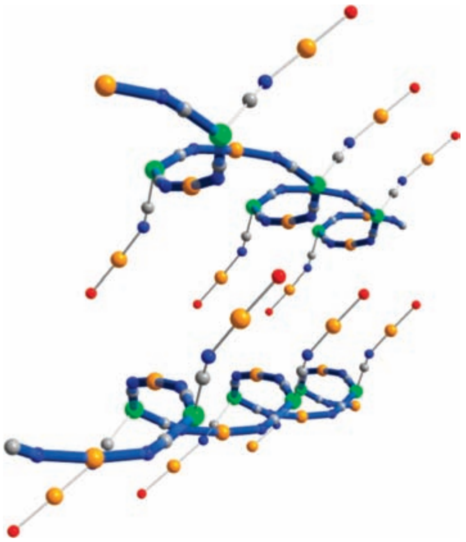

Figure 2. View of the right- and left-handed helical chains running along *b* axis (Fe in orange and Mo/W in green). For clarity only the bridging CN and the H_2O coordinated to Fe1 are depicted.

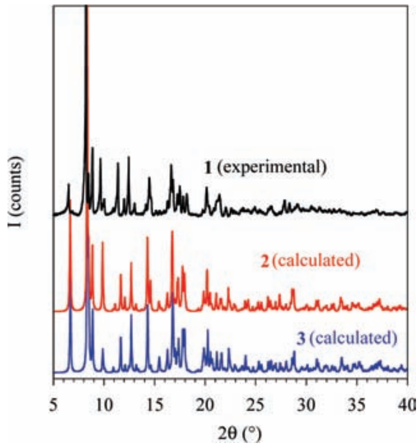

Figure 3. Experimental powder X-ray diffraction pattern for [{(H_2O)Fe($\mathbf{L^1}$)}{$Nb(CN)_8$}{Fe($\mathbf{L^1}$)}], **1**, compared to the pattern calculated for **2** and **3** from their crystal data. The unit cell parameters and space group obtained for **1** are $a = 13.649(7)$Å, $b = 17.537(7)$Å, $c = 20.976(8)$ Å, $\beta = 97.438°$, $V = 4973$ Å^3, space group = $P2_1/c$.

As mentioned above, the structure of the {Fe_2Nb} derivative **1** was confirmed by powder X-ray diffraction. The powder diffraction pattern (Figure 3), unit cell parameters, and space group obtained for **1** (see caption of Figure 3 and Supporting Information) match well with that found for compounds **2** and **3**, revealing isomorphous compounds.

---

(31) Note: cell parameters obtained for a single crystal of **1**: $a = 13.540$, $b = 17.963$, $c = 20.953$, $\beta = 99.8°$, V = 5021 cm^3.

(32) Drew, M. G. B.; Othman, A. H. B.; Nelson, S. M. *J. Chem. Soc., Dalton Trans.* **1976**, 1394–1399.

(33) Guionneau, P.; Sanchez Costa, J.; Létard, J.-F. *Acta Crystallogr. C* **2004**, *60*, m587–m589.

(34) Guionneau, P.; Marchivie, M.; Bravic, G.; Létard, J. F.; Chasseau, D. *Top. Curr. Chem.* **2004**, *234*, 97–128.

(35) Guionneau, P.; Gac, F. L.; Kaiba, A.; Costa, J. S.; Chasseau, D.; Létard, J.-F. *Chem. Commun.* **2007**, 3723–3725.

The polyhedral shape around the Mo and W centers do not correspond to ideal symmetry such as square antiprism, dodecahedron, or bicapped trigonal prism. Therefore a continuous shape measures (CShM) analysis[36−39] was carried out with SHAPE[40] to ascertain the actual geometry of the $\{M(CN)_8\}$ moieties. Indeed, the geometry of the $\{M(CN)_8\}$ polyhedron defines the strength of the exchange interaction mediated by each CN bridge.[21] Analysis of the coordination polyhedra of the cyanometalate core in chains **2** and **3** shows that the geometry around the metal center is distorted square antiprism. In this symmetry, all of the cyanide ligands are equivalent in mediating the magnetic interaction.[21] The results of the SHAPE analysis have been tabulated in Table SI4 in Supporting Information.

Mössbauer Spectroscopy. The hepta-coordinated $\{Fe(\mathbf{L}^1)\}$ unit was reported to exhibit an $S = 2$ spin state in the temperature range 90−300 K.[41] The possibility, at lower temperatures, of a spin conversion from $S = 2$ to $S = 1$ (high spin to low spin in a D_{5h} symmetry), as found for related compounds,[42] has been examined by Mössbauer studies undertaken for the Fe(II) complex and for the chain **3**. The Mössbauer spectra for $[\{Fe(\mathbf{L}^1)(H_2O)_2\}]Cl_2$ recorded at 80 and 5 K exhibit a unique well-resolved quadrupole-split doublet ($\delta = 1.148(6)$ mms^{-1}, $\Delta E_Q = 2.42(1)$ mms^{-1} at 5 K; $\delta = 1.174(5)$ mms^{-1}, $\Delta E_Q = 2.646(1)$ mms^{-1} at 80 K; see Supporting Information) that can be assigned to HS Fe^{II}.[43] For the chain **3** as well, the Mössbauer spectra confirm that the Fe centers remain high spin down to low temperature (Supporting Information). Interestingly, while spectrum for the $\{Fe_2W\}$ chain recorded at 5 K can been fitted by a unique resolved quadrupole-split doublet ($\delta = 1.15(4)$ mms^{-1}, $\Delta E_Q = 2.432(7)$ mms^{-1}), two quadrupole-split doublets ($\delta_1 = 1.13(3)$ mms^{-1}, $\Delta E_{Q1} = 2.59(5)$ mms^{-1}; $\delta_2 = 1.19(4)$ mms^{-1}, $\Delta E_{Q2} = 2.44(8)$ mms^{-1}) of similar area are found at 80 K. This is in agreement with the presence of two chemically nonequivalent Fe^{II} HS sites (terminal and *trans* NC coordinated) for which the quadrupole splittings differ slightly and which are also found in a 1:1 ratio through the X-ray analysis.[43] Obviously, both in the parent complex and in chain **3**, the Fe(II) unit remains high-spin with $S = 2$ down to cryogenic temperatures; magnetic properties (vide infra) will show that the same is valid for **1** and **2**.

Magnetic Properties. $[\{Fe(L^1)(H_2O)_2\}]Cl_2 \cdot 4H_2O$. The investigation of the magnetic behavior down to 2 K revealed a strong decrease of $\chi_M T$ (χ_M stands for the molar magnetic susceptibility) below 100 K with values of 3.36 and 1.85 cm^3 mol^{-1} K, respectively, at 300 and 2 K. Best fit of the Curie−Weiss equation to the experimental $1/\chi_M$ data yielded $\theta = -2.81$ K and $C = 3.41$ cm^3 mol^{-1} K. The field dependence of the magnetization was recorded at several temperatures between 2 and 10 K. At 2 K magnetization reaches a value of 2.3 μ_B at 50 kOe but does not saturate (4 μ_B is the saturation value expected for a $S = 2$ spin, taking $g = 2$) which suggests large anisotropy (the corresponding plots are provided as Supporting Information). The fit of the M versus *H/T* curves (Figure SI-5 in Supporting Information) was performed with the help of the MagProp program from the DAVE package[44] for the $S = 2$ spin Hamiltonian given in eq 1. It yielded $D = -17.2$ cm^{-1}, $E = 3.6$ cm^{-1}, considering a fixed isotropic g value of 2.12; these parameters have been used to model the $\chi_M T$ behavior for the compound (Figure SI-5 in Supporting Information). This large and negative D parameter is also supported by high-field EPR data (vide infra).

$$H = \mu_B \vec{S} \cdot \vec{g} \cdot \vec{H} + D\left[S_Z^2 - \frac{1}{3}S(S+1)\right] + E(S_x^2 - S_y^2) \qquad (1)$$

To characterize the anisotropic character of the $\{Fe(\mathbf{L}^1)\}$ unit, multifrequency high-field EPR experiments have been undertaken on a polycrystalline sample of $[\{Fe(\mathbf{L}^1)(H_2O)_2\}]Cl_2$. Two series of measurements have been performed with the Quasi-Optical setup,[45] one with the sample in a sealed EPR tube and the other with the sample in a Teflon cup. To avoid orientation by the magnetic field, the crystallites were mixed with paraffin in the first case and with grease in the second. In the frequency range from 95 to 345 GHz, only one low field resonance (Figure 4, left part) is observed (together with a $g \sim 2$ signal from an impurity). The resonance position, as well as its frequency dependence, is in agreement with the most intense signal expected for an $S = 2$ spin (Figure 4, right part) with the anisotropy determined from the magnetization measurements. As expected for a complex with very strong magnetic anisotropy ($|D| \sim 17$ cm^{-1}), very few signals are obtained even at high frequencies. The observation of a unique signal in the experimental spectra does not allow for a direct determination of the anisotropy parameters from the EPR study.

$[\{(H_2O)Fe(L^1)\}\{Nb(CN)_8\}\{Fe(L^1)\}]$, 1. The magnetic behaviors of the chains **1**−**3** have been investigated on polycrystalline samples. Only the results for $\{Fe_2Nb\}$ compound **1** is described below, the results for the Mo and W derivatives can be found in Supporting Information. For compound **1** the temperature dependence of the product of molar magnetic susceptibility, χ_M, and temperature in an applied field of $H = 100$ Oe is shown in log scale in Figure 5. The $\chi_M T$ product at 300 K is 7.6 cm^3 mol^{-1} K, in agreement with the paramagnetic contribution of two $S = 2$ $\{Fe(\mathbf{L}^1)\}$ ($g_{Fe} > 2.0$) and one $S = {}^1/_2$ spins. As the temperature is lowered, the $\chi_M T$ value gradually increases before it begins to rise steeply below 30 K to reach a value of 335 cm^3 mol^{-1} K at 6 K and then decreases to 133 cm^3 mol^{-1} K at 2 K. The field-cooled magnetization (FCM) tends to a plateau for the lowest temperatures investigated. When the applied field is switched off at 2 K, a remnant magnetization (REM) is observed. This REM drops rapidly and vanishes for T above 10 K. The same behavior is observed with an applied field of $H = 10$ Oe (Figure 5 insert), but with smaller magnetization values.

Theoretical Analysis of the Fe_2Nb Chain. Due to structural complexity and large size (average) of the Fe_2Nb chain, it is computationally challenging to model this system. In addition, since the experiment was done on a powder sample, chain axes

---

(36) Alvarez, S.; Alemany, P.; Casanova, D.; Cirera, J.; Llunell, M.; Avnir, D. *Coord. Chem. Rev.* **2005**, *249*, 1693–1708.

(37) Casanova, D.; Cirera, J.; Llunell, M.; Alemany, P.; Avnir, D.; Alvarez, S. *J. Am. Chem. Soc.* **2004**, *126*, 1755–1763.

(38) Casanova, D.; Llunell, M.; Alemany, P.; Alvarez, S. *Chem.—Eur. J.* **2005**, *11*, 1479–1494.

(39) Cirera, J.; Ruiz, E.; Alvarez, S. *Chem.—Eur. J.* **2006**, *12*, 3162–3167.

(40) Llunell, M.; Casanova, D.; Cirera, J.; Bofill, J. M.; Alemany, P.; Alvarez, S.; Pinsky, M.; Avnir, D. SHAPE, 1.1b; Barcelona, 2005.

(41) Drew, M. G. B.; Grimshaw, J.; McIlroy, P. D. A.; Nelson, S. M. *J. Chem. Soc., Dalton Trans.* **1976**, 1388–1394.

(42) Nelson, S. M.; McIlroy, P. D. A.; Stevenson, C. S.; Kñig, E.; Ritter, G.; Waigel, J. *J. Chem. Soc., Dalton Trans.* **1986**, *99*, 1–5.

(43) Greenwood, N. N.; Gibbs, T. C. *Mössbauer Spectroscopy*; Chapman and Hall: New York, 1971.

(44) Tregenna-Piggott, P. L. W.; Sheptyakov, D.; Keller, L.; Klokishner, S. I.; Ostrovsky, S. M.; Palii, A. V.; Reu, O. S.; Bendix, J.; Brock-Nannestad, T.; Pedersen, K.; Weihe, H. g.; Mutka, H. *Inorg. Chem.* **2009**, *48*, 128–137.

(45) Barra, A. L.; Hassan, A. K.; Janoschka, A.; Schmidt, C. L.; Schünemann, V. *Appl. Magn. Reson.* **2006**, *30*, 385–397.

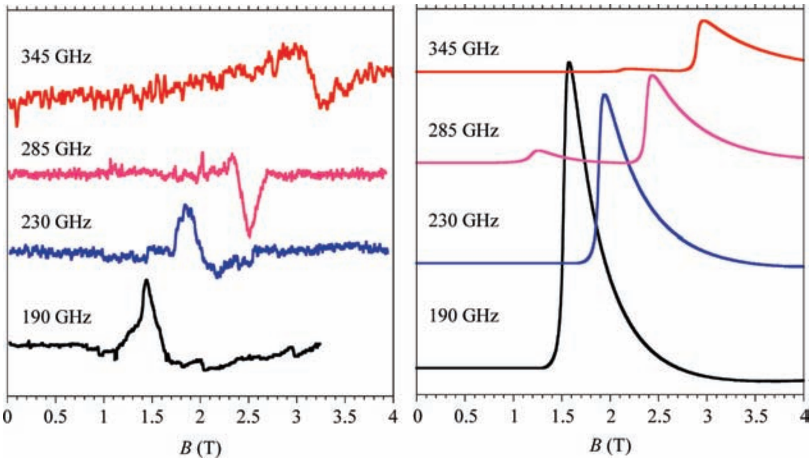

Figure 4. Experimental (left) and calculated (right) powder EPR spectra at frequencies of 190, 230, 285, and 345 GHz and at 5 K of the complex $[\{Fe(\mathbf{L^1})(H_2O)_2\}]Cl_2$. The experimental spectra are displayed after a baseline correction. The calculated spectra have been obtained for a $S = 2$ spin with the parameters indicated in the text.

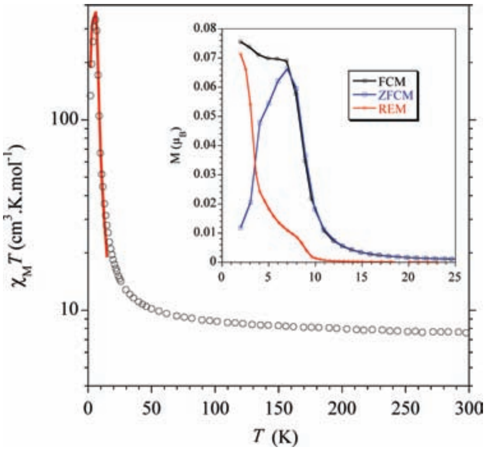

Figure 5. Temperature dependence of $\chi_M T$ (in log scale) for $[\{(H_2O)Fe(\mathbf{L^1})\}\{Nb(CN)_8\}\{Fe(\mathbf{L^1})\}]$, **1**, recorded with an applied field of $H = 100$ Oe. Solid lines represent the best fit to the experimental data obtained with the Ising model (red line) yielding $J_{NbFe} = -20.0$ cm^{-1}, $D = -16$ cm^{-1}, $g = 2.08$, $N = 140$ units (see text for details). Insert: related field-cooled (FCM), remnant (REM), and zero-field cooled (ZFC) magnetization recorded with $H = 10$ Oe (solid lines are guides for the eyes) (warming and cooling rate = 1 K·min^{-1}).

Scheme 1. One Structural Unit of the Fe_2Nb Chain[a]

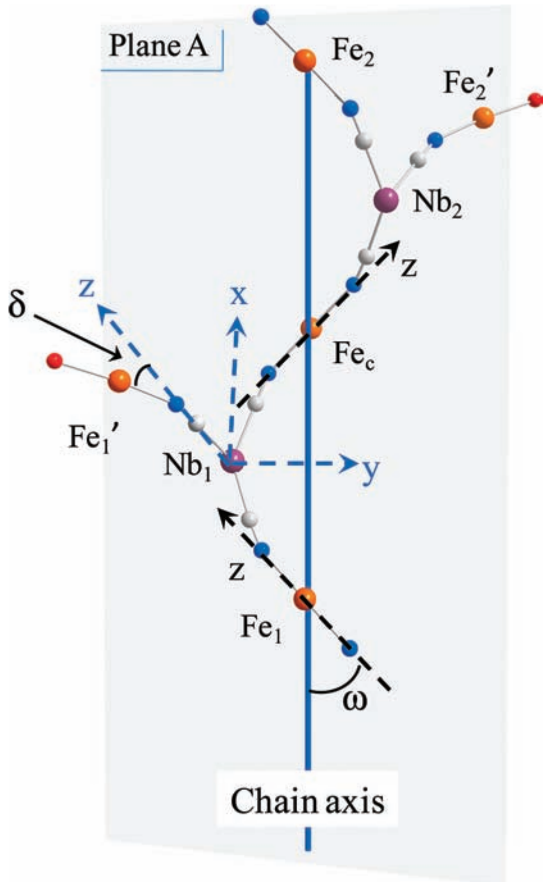

[a] ω is the angle made by the anisotropy axis (easy type) of in-chain Fe ions with the chain axis. δ is the angle between bonds Nb−C and N−Fe (off-chain); here it's just the angle made by the off-chain anisotropy axis with the local z-axis of Nb. α is the angle made by the local x-axis of Nb with the plane (A) formed by all alternate in-chain Fe ions (here Fe_1 and Fe_2) along with their anisotropy axes.

are oriented randomly in space; in principle one has to consider all possible orientations. For this (quasi) one-dimensional system, as the spin−spin correlation length at low temperature is assumed to be large (noting the huge value of χT at low temperature), we cannot take a few units of the chain to model the system. On the other hand, even after assuming iron spins to be Ising-like (due to their large axial anisotropy, whose estimation will be made from our modeling), we cannot use common transfer-matrix formalism for a one-dimensional Ising model. This is because Nb ions do not have anisotropy and all of their spin components are involved in exchange interactions. Since anisotropy axes of both in-chain and off-chain Fe ions are different and furthermore nearby Nb ions are not connected to the Fe ions in similar way, we here define three angles ω, α, and δ to describe the structure of the chain (Scheme 1). We also considered three coordinates θ, ϕ, and ψ to define the orientation of a chain, where θ and ϕ are the usual spherical polar coordinates to define the axis of the chain (the axis of the helix) and ψ here specifies the angle of rotation of the chain along its own axis. In this paper we concentrate on low-temperature modeling, as its property depends on exchange and anisotropy parameters along with structural angles. Physical insights into the system can be obtained by studying its low temperature properties. High temperature properties of a chain are easy to understand as all magnetic centers can be treated independently.

Low Temperature Modeling. If one carefully analyzes the chain structure, it can be seen that two chemical units (2 Fe_2Nb), which are connected by Fe ions, form one structural unit. Since at low temperature these Fe ions can be thought of as classical Ising spins, we can construct a two-dimensional transfer-matrix P that is a function of (i) temperature, (ii) all of the structural angles ω, α, and δ (specified above), and (iii) the magnetic field. It also depends on the angles θ, ϕ, and ψ, which define the chain orientation in space as the magnetic field experienced by magnetic ions depends on chain orientation in space. Therefore, for a given set of ω, α, and δ, we can obtain the partition function Q_N for N units as

$$Q_N(H,\beta;\theta,\varphi,\psi) = \lambda_1^N + \lambda_2^N \tag{2}$$

Here H is the magnetic field and $\beta = (1)/(k_BT)$ with k_B being the Boltzmann's constant. λ_1 and λ_2 are eigenvalues of the P matrix. Now since chains are oriented in all possible directions of space, we need to average out eq 2, to get average partition function $\bar{Q}_N(H,\beta)$ of a chain:

$$\bar{Q}_N(H,\beta) = \int_{\theta=0}^{\pi}\int_{\varphi=0}^{2\pi}\int_{\psi=0}^{2\pi} Q(H,\beta;\theta,\varphi,\psi)\sin\theta\, d\theta\, d\varphi\, d\psi \tag{3}$$

We ignored a normalization constant, as it will not affect our result. $\bar{Q}_N(H,\beta)$ is obtained for a different set of Hamiltonian parameters J and g for a chosen ω, α, and δ to find the best fitting. The formula we can use here for fitting the χ_MT versus T at low temperature is

$$\chi T = \frac{N_A k_B T^2}{2N}\frac{\partial^2}{\partial H^2}\ln \bar{Q}(H,\beta) \tag{4}$$

where N_A is Avogadro's number. To see the form of the P matrix, see Supporting Information. The best fit χ_MT versus T curve (Figure 5) gives $J = -20.0$ cm^{-1} (antiferromagnetic), $g = 2.08$, and $N = 70$ (hence 140 chemical units). Estimated D-value is -16 cm^{-1} (see Supporting Information). The best fit structural parameters are $\alpha = 34°$, $\omega = 22.5°$, and $\delta = 8°$. We note that at high temperature the theoretical curve gives a lower χT value than the experimental value. This is because, unlike the real system where magnetic ions at high temperature become independent and can align along the magnetic field irrespective of their anisotropy axis directions, in our model system no Fe ion can align along directions other than its own anisotropy axis. As a result this model cannot give maximum magnetization seen in the real quantum system. Another feature here worth mentioning is that, like experimental χT versus T curve, our modeling also gives a finite peak. Though it could not reproduce the experimental curve exactly below 6 K, it clearly shows the experimental trend of falling χT due to finite size of chains. This behavior of χT versus T indicates that correlation length saturates at about 6 K, below which correlation length becomes larger than the average chain length of 140 chemical units. The experimental energy gap of correlation length Δ_ξ from the ln(χT) versus 1/T plot is determined to be 33 K compared to the theoretical value of 34.5 K (see Supporting Information). The large value of χT at low temperature shows the 1-dimensional nature of compound **1**. Whereas good agreement of theoretical Δ_ξ, obtained by creating a domain wall in the chain, shows the possibility of slow relaxation in our compound by Glauber's dynamics. We indeed observe slow relaxation by AC susceptibility studies.

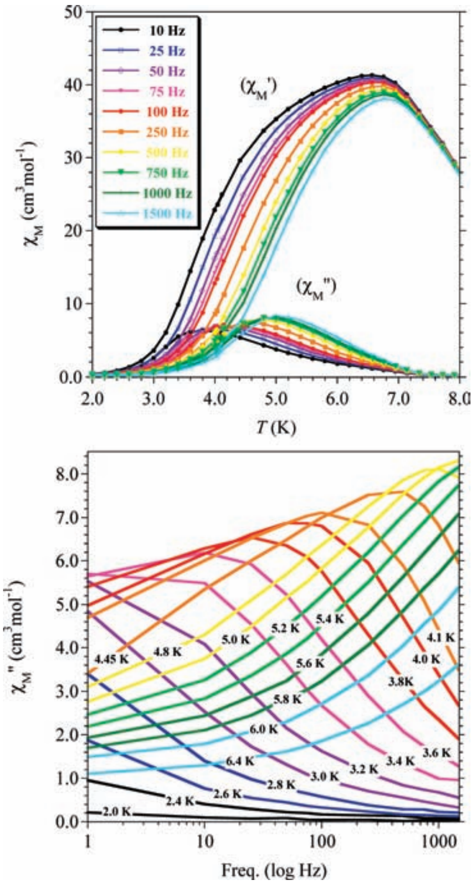

Figure 6. (Top) Temperature dependence of χ_M' and χ_M'' as a function of the frequency for [{(H_2O)Fe($\mathbf{L^1}$)}{Nb$(CN)_8$}{Fe($\mathbf{L^1}$)}], **1**. (Bottom) Frequency dependence of χ_M''. Measures have been made with zero applied static field and with an oscillating field of 3 Oe. Frequency dependences of the susceptibilities have been collected with static temperature.

The overall antiferromagnetic {Nb−Fe} interaction found for **1** is in agreement with earlier observations[46] and confirms an exchange pathway involving both σ- and π-type magnetic orbitals on the Fe center and the magnetically active π-orbitals of the cyanide bridges.[21,47,48] Its strength is in line with that found between {Nb$(CN)_8$} in square antiprism shape and the d^5 high-spin Mn^{II} ions.[49]

AC Susceptibility Studies. A series of AC susceptibility measurements were carried out for compound **1**. The measurements were made with zero applied static field and with an oscillating field of 3 Oe at 11 frequencies varying from 1 to 1500 Hz. In Figure 6, both the temperature and the frequency dependencies for the real part, χ_M', and the imaginary part, χ_M'', of the AC susceptibility are plotted.

The magnitude of the susceptibility at the maximum near 6 K is very large, indicating an enhancement of the susceptibility due to the ferrimagnetic arrangement of the spins along the chain. However, the magnitude of the applied susceptibility at the maximum is still more than 10 times less than what would

---

(46) Arai, M.; Kosaka, W.; Matsuda, T.; Ohkoshi, S. *Angew. Chem., Int. Ed.* **2008**, *47*, 6885–6887.

(47) Verdaguer, M.; Bleuzen, A.; Marvaud, V.; Vaissermann, J.; Seuleiman, M.; Desplanches, C.; Scuiller, A.; Train, C.; Garde, R.; Gelly, G.; Lomenech, C.; Rosenman, I.; Veillet, P.; Cartier, C.; Villain, F. *Coord. Chem. Rev.* **1999**, *190−192*, 1023–1047.

(48) Kahn, O. *Molecular Magnetism*; VCH: Weinheim, 1993.

(49) Venkatakrishnan, T. S.; Rajamani, R.; Ramasesha, S.; Sutter, J. P. *Inorg. Chem.* **2007**, *46*, 9569–9574.

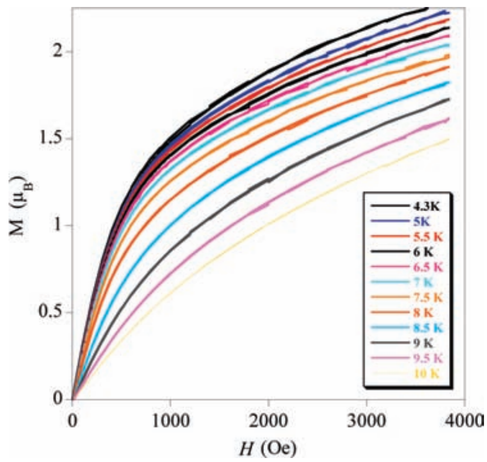

Figure 7. A series of isothermal M versus H curves near the peak in the susceptibility in Figure 6. The initial slope of the magnetization versus field tends to saturate below 6 K; however, no indication of a spontaneous magnetization appears below this temperature.

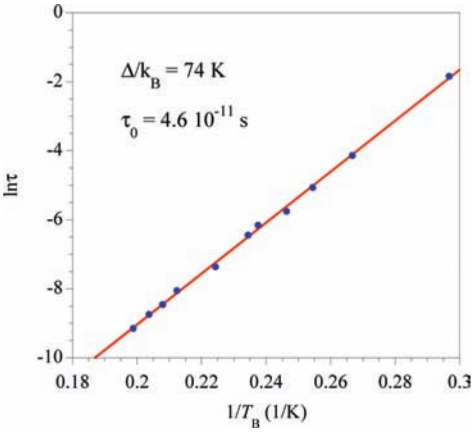

Figure 8. Plot of ln τ versus $1/T_B$, where T_B is the blocking temperature defined at the peak of χ'' for a given frequency ν and $\tau = 1/2\pi\nu$. The straight line is a fit to the data points.

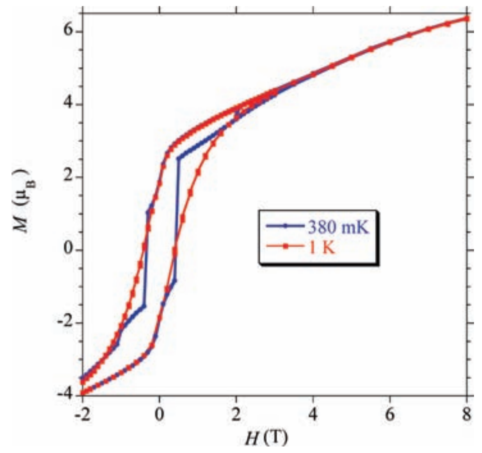

Figure 9. Hysterisis cycles of M versus H for **1** at 1 K and at 380 mK in fields up to ±8 T.

be expected at a ferromagnetic transition for a powder sample. To further rule out a phase transition, we looked at the behavior near the maximum by carrying out a series isothermal M versus H measurements below 10 K, as shown in Figure 7. As can be seen in the figure, although the initial slope of the magnetization versus field tends to saturate below 6 K, no indication of a spontaneous magnetization appears below this temperature. Indeed, an Arrott plot of this data shows no straight lines that can be attributed to a critical region,[50] and we can thus rule out a ferromagnetic phase transition for this sample. It can be mentioned that the isostructural $\{Mn_2Nb\}$ chain does not undergo 3D magnetic ordering down to 2 K.[27]

On the other hand, strong frequency dependence of the magnetization below approximately 8 K is evident from Figure 6. Below this temperature relaxation times become increasingly longer, and for a given frequency, a rather broad maximum in the imaginary part of the susceptibility occurs at a blocking temperature T_B, which shifts to lower temperatures for lower frequencies. This is the expected behavior of SCM: as the temperature is lowered, correlations along the chain grow, and it becomes more difficult for the spins to follow the field. χ_M' decreases, and a peak in the imaginary part χ_M'' of the susceptibility occurs below the maximum in χ_M'. In Figure 8 we plot the blocking temperatures (defined as the peak of χ_M'' for a given frequency) as ln τ versus $1/T_B$ where $\tau = 1/2\pi\nu$ is the corresponding relaxation time for a given frequency ν. The straight line is a fit to the data points and is a signature of thermal activation taking place following the Arrhenius law: $\tau = \tau_0 \exp \Delta/k_BT$. The values we obtained from the least-squares fitting are $\Delta/k_B = 74$ K and $\tau_0 = 4.6 \times 10^{-11}$ s. These parameters are in the range of those reported for SCMs and confirm that **1** exhibits an energy gap for the magnetization reversal.[1,2,6,51−54] Most important, however, is that the energy barrier for **1** is much larger than those known for octahedral Fe(II)-based SCMs .[55−57]

At even lower temperatures, the spins become effectively frozen. Below approximately 2.5 K and in high magnetic fields, the field dependence of the magnetization for chain **1** shows the opening of a hysteresis loop. Figure 9 shows two cycles measured at 1 K and at 380 mK in fields up to 8 T. The hysteresis cycle measured at 1 K is smooth, and the coercive field, H_C, is 0.4 T. On the other hand, at 380 mK, M versus H is not smooth; rather there are avalanches[58] or abrupt reversals in the magnetization as the field is varied, showing a martensitic-like nature for this sample at low temperature.

At the highest field 8 T and even at 380 mK, magnetization of compound **1** remains unsaturated, which indicates the anomalously large anisotropy for these chains. Similarly, saturation is not reached for compounds **2** and **3** (see Figure SI-6 in Supporting Information), where only Fe(II) in same

---

(50) *Introduction to the Theory of Ferromagnetism*; Oxford University Press: Oxford, 1996.

(51) Lescouëzec, R.; Vaissermann, J.; Ruiz-Pérez, C.; Lloret, F.; Carrasco, R.; Julve, M.; Verdaguer, M.; Dromzee, Y.; Gatteschi, D.; Wernsdorfer, W. *Angew. Chem., Int. Ed.* **2003**, *42*, 1483–1486.

(52) Miyasaka, H.; Clérac, R.; Mizushima, K.; Sugiura, K.; Yamashita, M.; Wernsdorfer, W.; Coulon, C. *Inorg. Chem.* **2003**, *42*, 8203–8213.

(53) Wang, S.; Zuo, J. L.; Gao, S.; Song, Y.; Zhou, H.-C.; Zhang, Y.-Z.; You, X.-Z. *J. Am. Chem. Soc.* **2004**, *126*, 8900–8901.

(54) Toma, L. M.; Lescouëzec, R.; Pasan, J.; Ruiz-Pérez, C.; Vaissermann, J.; Cano, J.; Carrasco, R.; Wernsdorfer, W.; Lloret, F.; Julve, M. *J. Am. Chem. Soc.* **2006**, *128*, 4842–4853.

(55) Kajiwara, T.; Nakano, M.; Kaneko, Y.; Takaishi, S.; Ito, T.; Yamashita, M.; Igashira-kamiyama, A.; Nojiri, H.; Ono, Y.; Kojima, N. *J. Am. Chem. Soc.* **2005**, *127*, 10150–10151.

(56) Przybylak, S. W.; Tuna, F.; Teat, S. J.; Winpenny, R. *Chem. Commun.* **2008**, 1983–1985.

(57) Tanaka, H.; Kajiwara, T.; Kaneko, Y.; Takaishi, S.; Yamashita, M. *Polyhedron* **2007**, *26*, 2105–2109.

(58) Minguet, M.; Luneau, D.; Lhotel, E.; Villar, V.; Paulsen, C.; Amabilino, D. B.; Veciana, J. *Angew. Chem., Int. Ed.* **2002**, *41*, 586–589.

environment is present. Nevertheless we can estimate the saturation value from inspection of Figure 9 as follows: Because these measurements were made on a powder sample, all orientations of the sample are measured at once and averaged in the figure. At low field, each individual small crystallite in the sample saturates rapidly along its own easy axis of magnetization, and correspondingly the magnetization increases rapidly and reaches a value of approximately 3.5 μ_B at 2 T. However as the field is increased further, the spins grudgingly start to align with the field against the local anisotropy, and evidently a field larger than 8 T is needed to align the magnetization of those crystals that are almost perpendicular to the field. Notwithstanding, for a powder consisting of a completely randomly orientated ensemble of crystallite axes, the magnitude at 2 T would correspond to one-half the expected saturation value of a crystal if it was perfectly aligned along the easy axis. This would imply a saturation value of 7 μ_B, which seems reasonable upon close inspection of Figure 9. More importantly, this would in turn imply that the two Fe $S = 2$ ions have antiferromagnetic interactions with the $S = {}^1/_2$ Nb ion, giving rise to a net spin 7/2 (assuming $g = 2$) and a ferrimagnetic chain.

The magnetic behavior exhibited by the {Fe_2Nb} chain, **1**, and especially the AC studies are consistent with a slow relaxation of the magnetization at low temperature. Such a behavior was not observed for the isostructural {Mn_2Nb} chain,[27] which underlines the prominent role of the anisotropic metal ion. The rather high energy barrier for the magnetization reversal, $\Delta/k_B = 74$ K, found for **1** can be certainly ascribed to the large and negative zero field splitting exhibited by the heptacoordinated Fe center as well as an efficient organization of the local uniaxial anisotropy of the Fe units throughout the chain. It can be stressed that observed energy gap of relaxation (74 K) is larger than energy gap of correlation length (33 K). The larger value of the energy barrier of relaxation can be attributed to the contribution from anisotropic Fe ions.

However, the dynamic susceptibility is not what one would expect from an ideal SCM. Indeed, analysis of the frequency data by using a Cole–Cole plot does show a rather broad distribution of relaxation times. This might be attributed to polydispersity of the chain lengths and/or to weak interchain interactions giving rise to some local short-range order. Interchain interaction is not contradictory with observation of slow relaxation dynamics for the chains that have been found even in ordered systems.[8,59] It has also been suggested that the chain topology may play a crucial role in both the SCM characteristics and the propensity of the material to undergo magnetic ordering.[60] For a helical organization such as in compound **1**, the noncolinearity of the anisotropy axes of the adjacent Fe centers is anticipated to reduce dipolar interactions and, subsequently, the ease for 3D magnetic ordering.

On the basis of the observations we have made here for static (from χT versus T curve) and dynamic (slow relaxation of magnetization) properties, it can be inferred that compound **1** exhibits a behavior reminiscent of a single-chain magnet.

Concluding Remarks. Substantial anisotropy in conjunction with high spin states of the repeating unit leads to an energy barrier that prevents or at least freezes reversal of the magnetization in low dimensional architectures. Hitherto, the different single-chain magnets reported are mainly based on Mn^{III}, Fe^{III}, Co^{II}, or lanthanides, which are known to exhibit significant single-ion anisotropy. The results reported here show that moving from octahedral to less conventional coordination geometries (heptacoordination in the present case) might be a valuable way to increase the anisotropy of paramagnetic transition metal complexes and hence attain improved magnetic behaviors for SCMs and related systems.

A further requirement to increase the energy barrier (Δ) for the magnetization reversal is substantial exchange coupling among the spin carriers throughout the chain. This has been achieved with the magnetic linker, $\{Nb(CN)_8\}^{4-}$. The choice of the 4d ion is based on the larger spin transfer from the metal to the ligands in the case of heavier ions, resulting in stronger exchange coupling. The reported compound is also among the first examples of a cyano-bridged Fe(II)–Nb(IV) system.[46,61] It revealed that for Fe in a D_{5h} environment an overall antiferromagnetic interaction results between these ions.

From a chemical point of view, consistent with our previous observation, the incorporation of a pentadentate macrocyclic ligand as blocking ligand around the 3d metal ion affords 1D architectures upon assembling with $\{M(CN)_8\}^{4-}$ ($M = Mo^{IV}$, Nb^{IV}, W^{IV}). This allows a rational design for improving the magnetic properties by varying the 3d metal ion and/or the octacyanometalate without affecting the supramolecular organization. More importantly, this unusual hepta-coordination contributes to the remarkable anisotropy exhibited by the Fe(II) unit. This opens interesting perspectives for designing new strongly anisotropic paramagnetic metal complexes that can be involved in the design and construction of magnetic architectures with desirable properties.

Experimental Section

The compounds $K_4[M(CN)_8]$ (M = Nb,[62] Mo,[63] and W[64]) were prepared by reported procedures. The materials $Na_2S_2O_4$, 2,6-diacetyl pyridine, triethylene tetramine, and $FeCl_2 \cdot 4H_2O$ were purchased from commercial sources. The solvents used in the reactions were degassed or distilled under a nitrogen atmosphere, and synthesis and manipulations of the solids were also performed in N_2 atmosphere. Infrared spectra were recorded in KBr pellets in the range 4000–400 cm^{-1} by using a Perkin-Elmer spectrum GX 2000 FTIR spectrometer. Elemental analyses were performed using Perkin-Elmer 2400 series II instrument.

Magnetic measurements down to 2 K were carried out with a Quantum Design MPMS-5S SQUID susceptometer. The low temperature susceptibility and magnetization measurements were made using two SQUID magnetometers developed at the MCBT, Institut Neel. One of the magnetometers is equipped with an 8 T superconducting magnet, whereas the other is designed for low field measurements (<0.2 T). Both use miniature dilution refrigerators capable of cooling samples down to 70 mK. Absolute values of the magnetization are made by the extraction method. A powder sample of approximately 2 mg was prepared by first mixing the sample in vacuum grease, and placing it inside a small Cu pouch, which was then fixed to the Cu sample holder attached to the bottom of the mixing chamber of the dilution refrigerator. Care was taken not to expose the sample to air during the preparation. All magnetic investigations were performed on polycrystalline samples mixed in grease and held in gelatin capsules. The molar susceptibility was

---

(59) Lhotel, E.; Khatsko, E. N.; Paulsen, C. *Phys. Rev. B* **2006**, *74*, 020402.

(60) Sessoli, R. *Angew. Chem., Int. Ed.* **2008**, *47*, 5508–5510.

(61) Pinkowicz, D.; Podgajny, R.; Pelka, R.; Nitek, W.; Balanda, M.; Makarewicz, M.; Czapla, M.; Zukrowski, J.; Kapusta, C.; Zajac, D.; Sieklucka, B. *Dalton Trans.* **2009**, 7771–7777.

(62) Kiernan, P. M.; Griffith, W. P. *J. Chem. Soc., Dalton Trans.* **1975**, 2489–2494.

(63) Leipoldt, J. G.; Bok, L. D. C.; Cilliers, P. J. *Z. Anorg. Allg. Chem.* **1974**, *409*, 343–344.

(64) Leipoldt, J. G.; Bok, L. D. C.; Cilliers, P. J. *Z. Anorg. Allg. Chem.* **1974**, *407*, 350–352.

corrected for the sample holder and for the diamagnetic contribution of all of the atoms by using Pascal's tables.[48]

Mössbauer measurements were recorded on a constant acceleration conventional spectrometer with a 50 mCi source of ^{57}Co (Rh matrix). The absorber was a powdered sample enclosed in a 20 mm diameter cylindrical, plastic sample holder, the size of which had been determined to optimize the absorption. Variable-temperature spectra were obtained in the 5−80 K range, by using an MD 306 Oxford cryostat, the thermal scanning being monitored by an Oxford ITC4 servocontrol device (0.1 K accuracy). A least-squares computer program was used to fit the Mössbauer parameters and determine their standard deviations (given in parentheses). Isomer shift values (δ) are relative to iron foil at 293 K.[65]

High-frequency EPR spectra were recorded at the Grenoble High Magnetic Field Laboratory on a home-built spectrometer working in single-pass mode, at 5 and 15 K. Gun diodes operating at 95 or 115 GHz, equipped with a frequency doubler or a frequency tripler, were used as excitation source. A Quasi-Optical table propagates the exciting light outside the cryostat, whereas a corrugated waveguide is used for this purpose inside the cryostat. A small modulating field is added to the main magnetic field in order to measure the derivative of the light transmitted through the sample. The detection is performed with hot electron InSb bolometer.

Synthesis of [$(H_2O)_2Fe(L^1)$]$Cl_2\cdot4H_2O$. The synthetic route adopted for the preparation of this complex is similar to that used for other Fe^{II} complexes bearing the same ligand with different counteranions;[41] however, isolation of the dicationic dichloro complex had not been reported earlier. $FeCl_2\cdot4H_2O$ (1.00 g, 5.03 mmol) was dissolved in a mixture of methanol (50 mL) and water (15 mL) under nitrogen atmosphere. To this solution were added $Na_2S_2O_4$ (0.438 g, 2.52 mmol), 2,6-diacetyl pyridine (0.821 g, 5.03 mmol) and triethylene tetramine (0.736 g, 5.03 mmol), and the dark blue reaction mixture was heated to 70 °C for 16 h. The reaction mixture was subsequently cooled to ambient temperature and filtered under nitrogen atmosphere to an aqueous (25 mL) solution of $Na_2S_2O_4$ (0.219 g). The dark blue mother liquor containing the compound was evaporated, and the resulting deep blue compound was redissolved in methanol (20−25 mL), concentrated to around 15 mL, and kept in a refrigerator leading to a dark blue crystalline compound. Large rectangular prismatic single crystals of the compound suitable for X-ray diffraction were grown from a dilute water−methanol solution in a refrigerator. The single-crystal X-ray structure was solved to establish the structural identity of the building block. The structure is similar to that of other complexes bearing the same ligand. Hence a detailed description of structure is not given. Full details of data are presented in Supporting Information in CIF format. Yield 1.820 g (75%); IR (KBr, cm^{-1}) 3422, 1651, 1590. Anal. Calcd for $C_{15}H_{32}N_5O_{4.5}FeCl_2$: C 37.44, H 6.70, N 14.55. Found: C 37.48, H 5.34, N 13.90.

Synthesis of [{$(H_2O)Fe(L^1)$}{$Nb(CN)_8$}{$Fe(L^1)$}]$_n\cdot4.5H_2O$, 1. $K_4[Nb(CN)_8]\cdot2H_2O$ (25 mg, 0.05 mmol) was dissolved in water (10 mL). Fe**L**^{1}Cl$_2$ (40 mg, 0.10 mmol) in a 1:1 mixture of H_2O and ethanol (15 mL each) was layered on top of the solution, and the mixture left for crystallization in dark. Well-formed blue-green crystals were obtained after 2 weeks along the sides of the tube. The crystals were isolated, washed with water, ethanol, and ether, and dried briefly in vacuo to obtain the pure compound. Yield 8 mg (15%); IR ν_{CN} (KBr, cm^{-1}) 2133, 2123, 2110. Anal. Calcd for $C_{38}H_{54}N_{18}O_4Fe_2Nb$: C 44.25, H 5.28, N 24.44. Found: C 44.55, H 5.23, N 24.06.

Synthesis of [{$(H_2O)Fe(L^1)$}{$Mo(CN)_8$}{$Fe(L^1)$}]$_n\cdot5H_2O$, 2. $K_4[Mo(CN)_8]\cdot2H_2O$ (45 mg, 0.09 mmol) was dissolved in water (8 mL). Fe**L**^{1}Cl$_2$ (72 mg, 0.18 mmol) in a 1:1 mixture of H_2O and ethanol (8 mL each) was layered on top of the solution and the mixture left for crystallization in dark at ambient temperature. Well-formed blue-green crystals suitable for X-ray diffraction were seen after 1 week along the sides of the tube. The crystals were isolated, washed with water, ethanol, and ether, and dried briefly in vacuo to obtain the pure compound. Yield 48 mg (51%); IR ν_{CN} (KBr, cm^{-1}) 2130, 2122, 2113, 2104. Anal. Calcd for $C_{38}H_{60}N_{18}O_7Fe_2Mo$: C 41.93, H 5.55, N 23.16. Found: C 41.87, H 5.30, N 22.94.

Synthesis of [{$(H_2O)Fe(L^1)$}{$W(CN)_8$}{$Fe(L^1)$}]$_n\cdot3.5H_2O$, 3. $K_4[W(CN)_8]\cdot2H_2O$ (58 mg, 0.10 mmol) was dissolved in water (12 mL). Fe**L**^{1}Cl$_2$ (80 mg, 0.20 mmol) in a 1:1 mixture of H_2O and ethanol (15 mL each) was layered on top of the solution and the mixture left for crystallization in dark. Well-formed blue-green crystals suitable for X-ray diffraction were seen after three weeks along the sides of the tube. The crystals were isolated, washed with water, ethanol, and ether, and dried briefly in vacuo to obtain the pure compound. Yield 38 mg (34%); IR ν_{CN} (KBr, cm^{-1}) 2128, 2120, 2112, 2101. Anal. Calcd for $C_{38}H_{52}N_{18}O_3Fe_2W$: C 41.32, H 4.75, N 22.83. Found: C 41.33, H 4.51, N 22.28.

X-ray Crystallography. A crystal suitable for diffraction was coated with paratone and mounted onto the goniometer, and intensity data was obtained from XCALIBUR Oxford CCD diffractometer using MoKα radiation (0.71073 Å) at 180 K for **2** and at 110 K for [$(H_2O)_2Fe(L^1)$]$Cl_2\cdot4H_2O$ employing φ and ω scans. The data for **3** was collected on STOE IPDS diffractometer employing φ scans.[66] The unit cell parameters were obtained by means of a least-squares refinement performed on a set of 8928 (**2**) or 8000 (**3**) well-measured reflections. The structures have been solved by direct methods using SIR92[67] and refined by means of least-squares procedures on *F* using the PC version of the program CRYSTALS.[68] The atomic scattering factors were taken from International Tables for X-ray Crystallography.[69] Absorption correction was performed using the multiscan procedure. Because of the limited number of reflections for compounds **2** and **3** only the heavy atoms were refined with anisotropic displacement parameters. Hydrogen atoms in **2** and **3** were introduced at calculated positions in the last refinement and refined by using a riding model. The hydrogen atoms in the complex [$(H_2O)_2Fe(L^1)$]$Cl_2\cdot4H_2O$ were located from the difference Fourier maps and were allowed to refine. Selected bond distances and angles are given in Supporting Information (Tables SI1−SI3).

Crystallographic Details for [$(H_2O)_2Fe(L^1)$]$Cl_2\cdot4H_2O$: ($C_{15}H_{35}N_5O_6FeCl_2$); $M = 508.23$, crystal size 0.60 mm × 0.35 mm × 0.20 mm, system, space group monoclinic, $P2_1/n$, $a = 10.9625(5)$ Å, $b = 8.5221(4)$ Å, $c = 24.6537(9)$ Å, $\beta = 95.801(4)°$, $V = 2292.4(2)$ Å^3, $Z = 4$, $T = 110$ K, $\rho_{calcd} = 1.473$ g cm^{-3}, $F(000) = 1072$, $\mu = 0.931$ mm^{-1}. A total of 19 793 reflections were measured in the range $2.91° \leq \theta \leq 29.17°$, of which 6146 were unique ($R_{int} = 0.03$). Final *R* indices: $R_1 = 0.0313$ [$I/2\sigma(I)$], $wR1 = 0.0849$; max/min residual electron density 0.677/−0.698 e Å^{-3}.

Crystallographic Details for 2: ($C_{38}H_{58}N_{18}O_6Fe_2Mo$); $M = 1070.63$, crystal size 0.15 mm × 0.30 mm × 0.60 mm, system, space group monoclinic, $P2_1/c$, $a = 13.4352(5)$ Å, $b = 17.5900(10)$ Å, $c = 21.0784(8)$ Å, $\beta = 99.578(3)°$, $V = 4911.9(4)$ Å^3, $Z = 4$, $T = 180$ K, $\rho_{calcd} = 1.45$ g cm^{-3}, $F(000) = 2168$, $\mu = 0.896$ mm^{-1}. A total of 49 352 reflections were measured in the range $3.03° \leq \theta \leq 32.11°$, of which 4776 were unique ($R_{int} = 0.04$). Final *R* indices: $R_1 = 0.097$ [$I/3\sigma(I)$], $wR1 = 0.112$; max/min residual electron density 1.46/−0.79 e Å^{-3}.

Crystallographic Details for 3: ($C_{38}H_{55}N_{18}O_{4.5}Fe_2W$); $M = 1131.52$, crystal size 0.03 mm × 0.20 mm × 0.25 mm, system, space group monoclinic, $P2_1/c$, $a = 13.403(5)$ Å, $b = 17.532(5)$

---

(65) Lagarec, K. *Recoil; Mössbauer Analysis Software for Windows*; http://www.physics.uottawa.ca/_recoil; Ottawa.

(66) Note: The Stoe IPDS because of the fixed phi spindle does not allow easy access to the cusp of data along the mount axis. This is an instrumentation-based restriction, which the author has little control over.

(67) Altomare, A.; Cascarano, G.; Giacovazzo, C.; Guagliardi, A. *J. Appl. Crystallogr.* **1993**, *26*, 343–350.

(68) Betteridge, P. W.; Carruthers, J. R.; Cooper, R. I.; Prout, K.; Watkin, D. J. *J. Appl. Crystallogr.* **2003**, *36*, 1487–1487.

(69) *International Tables for X-ray Crystallography*; Kynoch Press: Birmingham, England, 1974; Vol. IV.

Å, $c = 21.084(5)$ Å, $\beta = 99.478(5)°$, $V = 4887(3)$ Å^3, $Z = 4$, $T = 180$ K, $\rho_{calcd} = 1.54$ g cm^{-3}, $F(000) = 2248$, $\mu = 2.99$ mm^{-1}. A total of 48 735 reflections were measured in the range $2.05° \leq \theta \leq 26.10°$, of which 2942 were unique ($R_{int} = 0.08$). Final R indices: $R_1 = 0.060$ [$I/2.3\sigma(I)$], $wR2 = 0.067$ (all data); max/min residual electron density 0.99/−1.39 e Å^{-3}.

The powder X-ray diffraction pattern was collected on a XPert Pro (Theta-Theta mode) Panalytical diffractometer with λ (Cu $K_{\alpha1}$, $K_{\alpha2}$) 1.54059 Å, 1.54439 Å. The sample was sealed in a capillary of 0.5 mm diameter. The extraction of peak positions for indexing was performed with the fitting program, available in the PC software package Highscore+ supplied by Panalytical. Pattern indexing was carried out by means of the program DICVOL, and the space group test was performed using the LeBail Algorithm, implemented in the Highscore+ package.

Acknowledgment. This work was supported by the Centre Franco-Indien pour la promotion de la Recherche Avancée/Indo-French Centre for the promotion of Advanced Research (Project 3108-3), by the French Research Agency (Agence Nationale de la Recherche, reference ANR-09-BLAN-0054-01) The authors thank Dr. L. Vendier (LCC) for her assistance in powder X-ray crystallography.

Supporting Information Available: X-ray crystallographic files in CIF format for [$(H_2\mathbf{O})_2$Fe($\mathbf{L}^1$)]Cl_2, chains **2** and **3**; ORTEP plots with numbering scheme, tables of selected bond distances and angles for the three compounds; results of SHAPE analysis, magnetic behaviors for [$(H_2O)_2$Fe($\mathbf{L}^1$)]Cl_2, chains **2** and **3**; Mössbauer data; details on modeling. This material is available free of charge via the Internet at http://pubs.acs.org.

JA9089389